Preprint: The Journal of Physical Chemistry C: https://doi.org/10.1021/acs.jpcc.0c04532

Electrochemical Decoration of Additively Manufactured Graphene Macroelectrodes with MoO_2 Nanowires: An Approach to Demonstrate the Surface Morphology

Anthony J. Slate[1,2,3], Kathryn A. Whitehead[1,3]*, Stephen Lynch[4], Christopher W. Foster[1], and Craig E. Banks[1,2]*

[1]: Faculty of Science and Engineering, Manchester Metropolitan University, Chester Street, Manchester, M1 5GD, UK.

[2]: Manchester Fuel Cell Innovation Centre, Manchester Metropolitan University, Chester Street, Manchester M1 5GD, UK.

[3]: Microbiology at Interfaces, Department of Life Sciences, Manchester Metropolitan University, Chester Street, Manchester M1 5GD, UK.

[4]: Department of Computing and Mathematics, Manchester Metropolitan University, Chester Street, Manchester M1 5GD, UK

The Journal of Physical Chemistry C

*To whom correspondence should be addressed.

Email: K.A.Whitehead@mmu.ac.uk (Proofs and correspondence); c.banks@mmu.ac.uk

Abstract

Additive manufacturing (AM) provides a unique platform for the rapid design and fabrication of complex structures. Printed structures can be used as is or as templates to be decorated with electrochemical deposited nanomaterials, which may be utilised as electrocatalytic sensing platforms. Novel methods are required to determine the electrochemical deposited morphology present on the electrode surfaces. Additively manufactured graphene macroelectrodes (AM-G_{MS}) were fabricated using a commercially available feedstock and molybdenum (di)oxide (MoO_2) was successfully electrochemically deposited onto the electrode surface. The electrochemically deposited MoO_2 was analysed using scanning electron microscopy (SEM), optical interferometry, Raman spectroscopy and multifractal analysis (MFA). Although the electrochemical deposition of MoO_2 nanowires were clearly visible using SEM, MFA enabled quantification of the MoO_2 nanowires, deposited at a variety of time points (20 – 300 s). MFA was utilised to generate quantitative data, derived from $f(\alpha)$ curves, to determine the area of the electrochemical deposited MoO_2 nanowires, including coverage, density, dispersion and clustering. The AM-G_{MS} which were subjected to 300 s (maximum time period) of MoO_2 electrodeposition demonstrated the greatest percentage area coverage (20.14 %). The use of such mathematical systems offers an inexpensive method to characterise the parameters of electrochemically-deposited materials.

Keywords: Additive Manufacturing; Graphene; MoO_2; Multifractal analysis; Macroelectrodes.

Introduction

Additive manufacturing (AM) is now routinely being used to fabricate advantageous electrochemical surfaces. The incorporation of 2D nanomaterials such as graphene[1,2] and carbon nanomaterials[3-5], into additive manufactured polymers has resulted in a wide range of interest, due to their combined superior physical and electrochemical properties in comparison to their macroscopic counterparts. An alternative approach currently being researched is the AM of an electrode as the basis/template, with nanomaterials then being electrochemically deposited onto the electrode surface, these electrodes can then be used as, for example, electrocatalytic electrochemical sensing platforms towards a range of target analytes[6,7].

The fabrication of graphene-based conductive filaments, consisting of polylactic acid (PLA) and acrylonitrile-butadiene-styrene (ABS), with graphene loadings of up to 5.6 wt.%, have been successfully AM, resulting in the production of macroelectrodes for potential application in next generation energy architectures[9]. Furthermore, studies utilising AM graphene macroelectrodes (AM-G_Ms) have been conducted[8,9]; in a study conducted whereby graphene-based polylactic acid (PLA) filaments were AM to fabricate a range of architectures, which were successfully applied as both, freestanding anodes (within Li-ion batteries) and solid-state capacitors[10]. The graphene/polylactic acid filament has also been AM into a base electrode material and the fabricated electrodes were sputtered with gold and utilised as solid-state supercapacitors, demonstrating promising capacitive performance and cycling stability over 100 charge/discharge cycles[11]. There is consequently a need to characterise the electrochemically deposited surface morphology. In this paper we AM graphene macroelectrodes (AM-G_Ms) and demonstrate a novel quantification technique to determine the area of electrochemically deposited MoO_2 nanowires upon AM-G_Ms. Molybdenum (di)oxide (MoO_2) was selected for utilisation in this study due to its wide negative potential working window, multiple valance states, excellent electrochemical activity, environmentally benign nature and low

cost[12-17]. Through the utilisation of MFA, the physical coverage of the electrodeposited MoO_2 was quantified, allowing the true area of the deposited material to be determined. This approach is useful for the determination and quality assurance of AM-G_Ms, which have both wide and diverse implications in a plethora of applications.

Experimental section

All chemicals (of analytical grade or higher) were used as received from Sigma-Aldrich without further purification. All solutions were prepared with deionised water of resistivity no less than 18.2 MΩ cm and were vigorously degassed prior to electrochemical measurements with high-purity, oxygen-free nitrogen. This degassing stage is of paramount importance, as it removes any trace oxygen, which if present could convolute the results acquired due to the oxygen reduction reaction (ORR) occurring[18].

Electrochemical measurements were conducted using a 'μAutolab Type III' (Metrohm Autolab, The Netherlands) potentiostat and data generated was collected and analysed using the software; NOVA (Version 2.0). All measurements were conducted using a typical three-electrode system. The working electrodes utilised throughout this study were additively manufactured (AM) Black Magic macroelectrodes (AM-G_Ms; see below), where a platinum wire and a saturated calomel electrode (SCE) were used as counter/auxiliary and reference electrodes, respectively.

Fabrication of the additively manufactured Graphene Macroelectrodes (AM-G_Ms)

The AM designs were fabricated using a MakerBot Replicator + (MakerBot Industries, USA) with a direct drive extruder at a temperature of 210 °C, using a commercially procured filament (Black Magic 3D, USA), which is a Graphene/PLA composite with a calculated conductivity of 2.13 S/cm[10] and a graphene content of 8 wt.%[10]. The AM designs were drawn *via* Fusion 360 (Autodesk, USA), to create a circular disc electrode architecture with a diameter of 6.0 mm and a thickness of 1.0 mm. The AM-G_Ms were printed with a connecting strip

allowing simple connection of the electrode to the electrochemical system *via* a crocodile clip[19]. The 3AM-G_Ms electrodes utilised in this study had a theoretical surface area of 0.75 cm^2, however, in order to compare the electrochemical analysis with the MFA analysis, one face of the electrode was isolated using Parafilm®, due to its flexibility and insulating properties[20,21]. Thus, a theoretical surface area of 0.282 cm^2 was utilised throughout this study.

The electrodeposition of MoO_2 on AM-G_Ms

A solution containing 1 mM sodium molybdate ($NaMoO_4$), in supporting 1 M sodium chloride (NaCl) and 1 M ammonium chloride (NH_4Cl) was prepared and adjusted to a pH of 8.5 with NH_4OH. Cyclic voltammetry was performed within the potential range of + 0.5 V to – 1.2 V at a scan rate of 5 mV s^{-1} (*vs*. SCE)[22]. On the cathodic sweep, MoO_2 deposition is evident *via* a reduction peak at *ca.* - 0.9 V to - 1.0 V. The average half peak potential of the reduction/deposition peak (-0.805 V (*vs*. SCE)) was then taken as the deposition value which was then utilised throughout this study (N = 6). Subsequently, this potential was held during chronoamperometry for varying time-points, namely, 20, 40, 60, 120, 180, 240 and 300 s in order to achieve successful deposition of MoO_2 nanowires upon the AM-G_Ms. Following chronoamperometry, the electrodes were rinsed gently with deionised water (as above) in order to remove excess salt residues. At each time-point, MoO_2 deposition was carried out in triplicate with 3 independent electrodes.

Surface characterisation

Prior to the MoO_2 electrodeposition process the topography of the isolated surfaces were measured using optical interferometry[23]. An AM PLA electrode (containing no graphene) was also evaluated in order to derive accurate comparisons. Surface roughness was quantitatively defined through the measurement of average roughness (S_a), highest peak (S_p), lowest valley (S_v) and the peak-to-valley ratio (S_{pv}), using a Zemetrics, Zegage 3D optical

profiler (Zygo, USA) at × 50 magnification. Zemaps (version 1.14.38) was the image analysis software used. Only samples that had > 90 % of the surface analysed were included ($N = 9$).

Scanning electron microscope (SEM) images were obtained using a JEOL JSM-5600LV model SEM with an accompanying energy dispersive spectrometer (EDS). Raman Spectroscopy was conducted using a 'Renishaw InVia' spectrometer, which was equipped with a confocal microscope (× 50 objective) and an argon laser (with an excitation wavelength of 514.3 nm). In order to prevent any potential heating effects, measurements were performed at a low laser power level (0.8 mW)[18,24].

Multifractal analysis (MFA) was carried out in a similar manner to that adopted by Wickens *et* al, 2014[25]. In order to observe the properties of typical multifractal spectra, datasets were constructed from a set of motifs of the SEM images obtained using MATLAB®[26], and theoretical and physical $f(\alpha)$ spectra were compared. Using an iterative program, datasets of size 512 × 512 pixels were computed by overlapping the given motifs on top of one another, thus, after one iteration a 4 × 4 matrix was formed, a second iteration leads to an 8 × 8 matrix, through until completion (Figure 1). Datasets were converted to greyscale images *via* the MathWorks Image Processing Toolbox®; in this converted scale a value of zero would give a black pixel and a value of one would give a white pixel[25,26]. It is important to note that the theoretical $f(\alpha)$ spectra generated in our recent paper exist for, $-\infty \leq q \leq \infty$, however, in physical applications the q values are usually restricted by physical constraints. In Figure 1, theoretical $f(\alpha)$ spectra are plotted with blue curves and numerical $f(\alpha)$ spectra are plotted with red pluses.

In this paper, the numerical $f(\alpha)$ spectra were computed for, $-10 \leq q \leq 10$, in all cases and dataset boxes of size, ε = 4, 8, 16, 32, 64, 128 and 256[25] were used in the computation. From this, the $f(\alpha)$ curves were generated and this enabled relative density, dispersion and

clustering of the MoO_2 nanowires to be computed. The maximum value of the $f(\alpha)$ curve (when $q = 0$):

$$D_0 = f(\alpha_0) \quad (1)$$

gives a numerical value for the density of MoO_2 upon the surface of the electrodes, whilst dispersion of the MoO_2 at the edge planes was measured by (2):

$$\Delta\alpha = \alpha_{-10} - \alpha_{10}. \quad (2)$$

The degree of MoO_2 clustering was established *via* the symmetry/antisymmetry of the generated $f(\alpha)$ curves[25] using the formula (3):

$$\Delta f(\alpha) = f(\alpha_{10}) - f(\alpha_{-10}). \quad (3)$$

A positive value of $\Delta f(\alpha)$ indicated clustering of MoO_2, whereas a negative value of $\Delta f(\alpha)$ indicated clustering of gaps (Figure 1). Independently of the $f(\alpha)$ curves, analysis of the images was also conducted to determine maximum area and the total MoO_2 percentage coverage[25,30]. The theory behind MFA theory and $f(\alpha)$ curves is described (Figure 1). The previously obtained SEM images (all at 15.00 K X) were analysed using MFA. Firstly, grey-scale images were converted to a binary format using image processing and MFA was carried out and the resultant computed curves were plotted. Following the acquisition of the $f(\alpha)$ spectra, quantitative outputs were calculated using equations (1)-(3).

Results and Discussion

Prior to the MoO_2 electrodeposition process, the surface roughness of the electrodes was evaluated utilising optical interferometry (Figure 2). This allowed comparisons of the AM-G_Ms to be derived against AM PLA (AM-PLA) electrodes, which were graphene deficient. The AM-G_Ms demonstrated the greatest average surface roughness (4.40 μm; PLA control (3.44 μm)), highest peak (13.86 μm; PLA control (10.99 μm)), lowest valley (-21.12 μm; PLA control (-13.81 μm)), and the peak-to-valley ratio (34.95 μm; PLA control (24.70 μm)). This indicates that the addition of graphene resulted in an enhanced surface topography; this phenomenon could be a direct

result of the agglomeration of graphene, which may protrude through the surface of the electrode, resulting in a less uniform topography than the PLA counterpart[10].

Cyclic voltammetry was utilised in order to establish an effective deposition potential that was utilised during the chronoamperometry studies, allowing for the adequate coating of the AM-G_Ms with MoO_2. An average half reduction peak potential was determined at -0.805 (± 0.002) V (*vs*. SCE) ($N = 6$). Subsequently, this potential was held during chronoamperometry to coat the AM-G_Ms with MoO_2 nanowires over varying deposition times, namely, 0, 20, 40, 60, 120, 180, 240 and 300 s. The above method has been adapted from Zach *et al*[27], Walter *et al*[22] and more recently Rowley-Neale *et al*[28] and Garcia-Miranda *et al*[29], whereby the cathodic sweep in the voltammograms reveals the deposition of the MoO_2 due to the reduction of Mo^{6+} to Mo^{4+} and this occurs *via* the following equation (4)[22,28]:

$$MoO_4^{2-} + 2H_2O + 2e^- \rightleftharpoons MoO_2 + 4OH^- \quad (4)$$

The above equation (4), at the appropriate potential (- 0.805 V (*vs*. SCE)) results in the nucleation and production of MoO_2 nanowires on the AM-G_Ms presented in this study. The inverse reaction, which is presented as an oxidation peak during the anodic sweep of the cyclic voltammograms, relates to the oxidation of MoO_2 on the surface on the electrode to MoO_4^{2-}, which is then re-dissolved into the solution. The maximum intensity of the reduction peak is observed at *ca.* - 0.95 V (*vs*. SCE), whilst the study carried out by Rowley-Neale *et al*, reported a maximum reduction peak intensity of *ca*. - 1.3 V (*vs*. SCE) utilising screen-printed graphite electrodes[28]. Previously, Walter *et al.* demonstrated that MoO_2 nanowire formation can be controlled by selecting specific parameters (such as deposition potential and time) upon a highly oriented pyrolytic graphite (HOPG) electrodes; at - 0.7 V (*vs*. SCE) this study reported that MoO_2 formation was exclusive to the edge planes, whilst at - 0.85 V (*vs*. SCE) a high degree of specificity was revealed but a small number of particles could be seen *via* SEM on the basal planes[22]. However, at - 1.25 V (*vs*. SCE), MoO_2 nucleation drastically increased on

the basal planes[22]. Subsequently, for this study, the average half peak potential of - 0.805 V (*vs*. SCE) was selected in order to ensure specificity to the electro-active regions (edge planes) only.

The AM-G_Ms coated with MoO_2 were subjected to independent surface characterisation specifically SEM, Raman spectroscopy and MFA. Evidence of MoO_2 deposition was determined *via* the utilisation of SEM (Figure 3). The SEM images acquired, revealed that the electrodes coated with MoO_2, for 20, 40 and 60 s demonstrated little variation from the control electrode. However, electrodes electrodeposited with MoO_2 for 120, 180, 240 and 300 s, exhibited the formation of MoO_2 nanowires. After a deposition time of 240 s the formation of filamentous nanowires was observed, specifically along the edge plane like-sites/defects planes. The nucleation of MoO_2, increased, with the AM-G_Ms coated for 300 s resulting in a thick nucleation on the edge planes of the electrode. For both the 240 s and 300 s time points, MoO_2 nanowires > 2 μm in length were observed (Figure 3).

To further validate the electrodeposition of MoO_2, Raman spectroscopy was performed on the AM-G_Ms over the eight varying deposition times. The Raman spectra of four selected MoO_2 deposition time points are displayed (Figure 4). The Raman spectra over eight varying deposition times are presented in Electronic Supplementary Information (ESI; Figure S1); whilst, the first 1000 cm^{-1} of Raman shift, due to the diversity in presence and intensity of peaks displayed in this region are also depicted (Figure S2). Each of the Raman spectra obtained in this study revealed carbonaceous characteristic peaks, commonly referred to as the G and 2D (G') bands at *ca.* 1580 cm^{-1} and 2690 cm^{-1}, respectively[30-34]. The spectra obtained in this study revealed that the graphene component of the AM-G_Ms was comprised of multi-layer graphene sheets, which was evidenced in the highly symmetrical 2D (G') band peak. Further, there was a distinct lack of the characteristic 'shoulder', which was observed in the case of graphite[30,35]. The large D band that was prominent in the Raman spectra's indicated a high

number of edge plane like-sites[36]. Full width half maximum (FWHM) analysis of the 2D bands, revealed the control AM-G_Ms demonstrated a Raman shift of 86.55 (± 0.98) cm^{-1}, whilst the FWHM of the 2D bands, of the AM-G_Ms subjected to MoO_2 deposition produced Raman Shift values in the range of 72.80 (± 1.07) cm^{-1} (300 s) – 103.96 (± 2.83) cm^{-1} (180 s). This was in agreement with Foster *et al*, (2017) who utilised the same AM-G_Ms and reported a FWHM value of 94 cm^{-1} (of the 2D peak), indicating agglomeration of the graphene in the PLA filament[10]. Therefore, the presence of multi-layered graphene was confirmed, as the FWHM values of the 2D band for monolayer graphene and *quasi*-layer graphene corresponded to 28 cm^{-1} and 58 cm^{-1}, respectively[37,38].

The MoO_2 coated AM-G_Ms of deposition times, 20, 40 and 60 s demonstrated three distinct peaks at *ca.* 404 cm^{-1}, 510 cm^{-1} and 630 cm^{-1}, respectively. However, these peaks were also evident on the control AM-G_Ms and therefore were assumed to be from the AM process. The AM-G_Ms that were electro-deposited with MoO_2 for 120 s, 180 s and 240 s demonstrated a distinct peak at *ca.* 281 cm^{-1}. Zhou *et al*, (2016) previously demonstrated a Raman spectra of MoO_2 nanoparticles, with characteristic peaks observed at *ca*. 287 cm^{-1}, 341 cm^{-1}, 666 cm^{-1}, 819 cm^{-1} and 987 cm^{-1}[39]. The peak at 287 cm^{-1} was observed at 120 s, 180 s and 240 s, whilst it could be suggested that other potential peaks demonstrated could be masked by the signals from the electrode material alone[39]. The AM-G_Ms that was exposed to MoO_2 deposition over 300 s, demonstrated that the Raman spectra observed in this instance demonstrated differences to the other time-points analysed. This may have been due to the build-up of the MoO_2 on the surface. Two new peaks were specific to this time point, observed at *ca.* 860 cm^{-1} and 960 cm^{-1}, providing further evidence of MoO_2 on the surface of the electrode which was in further agreement with Zhou *et al*, (2016)[39].

For image analysis and MFA to be conducted, the grey scale images obtained during SEM (at 15.00 K X) were converted to binary images (Figure S3), this resulted in the

production of $f(\alpha)$ curves to compute density, dispersion and clustering (Figure 5). Area coverage (percentage coverage) was also calculated, this revealed that the AM-G$_M$s coated with MoO_2 for the 20 s deposition rate which had the lowest coverage of MoO_2. An increase in percentage area cover was observed on the 120 s MoO_2 AM-G$_M$s (8.37 %). This increase was observed to be relatively linear (excluding the 180 s deposition time point – 19.34 %), with the 240 s and 300 s deposition time points demonstrating MoO_2 area coverage of 13.07 % and 20.14 %, respectively (Figure 5C). The $f(\alpha)$ curve (Figure 5B), results showed that the AM-G$_M$s coated with MoO_2 for 20 s produced the lowest density of the MoO_2 area coverage, $D_0 = 1.45$, whilst the AM-G$_M$s coated with MoO_2 for 300 s produced the greatest density, $D_0 = 1.75$. The dispersion of the MoO_2 area coverage was calculated which related to the heterogeneity of the MoO_2 nanowires present on a given area of the electrode surface. Dispersion, and hence heterogeneity, was highest for the AM-G$_M$s coated with MoO_2 for 20 s, $\Delta\alpha = 1.17$, and lowest for the AM-G$_M$s coated with MoO_2 for 300 s, $\Delta\alpha = 0.69$. Finally, clustering ($\Delta f(\alpha)$) of the MoO_2 nanowires were determined as per equation (3). Excluding the control AM-GMs (no MoO_2 deposition), the 20 s MoO_2 deposition time produced the highest clustering value (0.76). A $\Delta f(\alpha) > 1$, indicated a cluster of gaps and therefore more space between the MoO_2 on the surface of the electrode[25,40]. As the deposition time of MoO_2 increased, the clustering value became more negative, with the first negative value reported at 180 s (-0.055) and the most negative value was observed at the 300 s MoO_2 deposition time point. A $\Delta f(\alpha) < 1$ indicated more intense clustering of the MoO_2[25,40]. Therefore, MFA revealed that clusters of gaps were dominant up to 60 s, and that clusters of MoO_2 were observed for 240 s and 300 s, indicating a time-dependent deposition process. Interestingly, as the MoO_2 deposition time increased the MoO_2 on the AM-G$_M$s became more agglomerated, this strengthens the theory that the MoO_2 selectively bound to the electrochemically active sites of the AM-G$_M$s. Thus, MFA which relies upon the estimation of fractional features[41] was successfully used in this study, the fractional

features correlate to MoO_2 depositions. MFA has been applied in a wide array of biological and chemical fields, such as, disease diagnosis,[41] bacterial quantification and cell dispersion[25,42] and to evaluate the sensitivity of catalytic reactions to catalyst structure[43]. MFA has previously been shown as a method to characterise the topography of surfaces[44].

Table 1 lists the generalized fractal dimensions, D_q, corresponding to the $f(\alpha)$ curves displayed in Figure 5 B) for $-10 < q < 10$. A multifractal methodology is provided by Salat *et al.*,[45], where the formula for obtaining D_q from the $f(\alpha)$ curves is shown to be (5):

$$D_q = \frac{f(\alpha)-q\alpha}{1-q} \quad (5)$$

where $-\infty < q < \infty$. The generalized dimension, D_0, is the capacity (or box-counting) dimension and gives a measure of density. The elements, $D_{\pm 1}$, are known as the entropy (or information) dimensions and relate to Shannon's entropy giving a measure of how even/uneven the data density is. The other commonly used generalized fractal dimensions are, $D_{\pm 2}$, called the correlation dimensions, which relate to how scattered the data is. Table 1 shows that the quantities, D_0, $D_{\pm 1}$, and $D_{\pm 2}$, all increase as the deposition time points increase from 20 s up to 300 s. Higher values of $D_{\pm 1}$, imply a more uniform density and increasing values of $D_{\pm 2}$, imply increasing compactness. The full range of values of D_q versus q illustrates the strength of the multifractality of the data.

This study reports the utilisation of MFA to determine the percentage coverage, dispersion, density and clustering of MoO_2 on porous AM-G_Ms. Such analysis provides further insight and evidence of fundamental graphene electrochemical behaviour *via* the nucleation of MoO_2 nanowires. In light of these findings, it is suggested that this method can be utilised in order to effectively visualise and quantify the electrochemical active regions (such as edge plane sites/defects) of AM-G_Ms and other high surface area architectures.

Conclusions

In this study, the fabrication of MoO_2 nanowires onto AM-G_Ms has been demonstrated. SEM images demonstrated a time-dependent deposition process and the utilisation of MFA led to the generation of quantitative data (percentage area cover, clustering, density and dispersion) of the MoO_2 nanowires on the AM-G_Ms. This provided evidence that the MoO_2 selectively bound and accumulated (as seen by the clustering) to the electrochemically active sites of the AM-G_Ms. This technique has the potential to be applied to other carbonaceous macroelectrodes, regardless of the fabrication method, allowing electrochemical active regions to be appropriately benchmarked and characterised.

Supporting Information Description

The supporting information provides Raman spectra of the eight MoO_2 deposition time points against the AM-G_Ms, Raman spectra (focussing on the first 1000 cm^{-1}) of the eight MoO_2 deposition time points against the AM-G_Ms and examples of the binary images, which were generated and modified following SEM, before MFA was conducted.

Acknowledgement

This research was funded by the Manchester Metropolitan University. Funding from the Engineering and Physical Sciences Research Council is recognised (Reference: EP/N001877/1).

Author Information

Dr Anthony J. Slate (Postdoctoral Scientist), ajs319@bath.ac.uk

Professor Kathryn A. Whitehead (Professor in Microbiology at Interfaces)

K.A.Whitehead@mmu.ac.uk

Dr Stephen Lynch, (Reader and Deputy Head of Department, Computing and Mathematics),

S.Lynch@mmu.ac.uk

Dr Christopher W. Foster (Postdoctoral Scientist), cwfoster90@gmail.com;

Professor Craig E. Banks (Professor in Chemistry), c.banks@mmu.ac.uk

Author Contributions The concept behind the work was developed by KAW and CEB. The experimental methodology was developed and carried out by AJS, CWF and SL. The manuscript was written by AJS, SL, CEB and KAW. All the authors were involved in the final proofing of the manuscript.

Conflict of Interest. The authors declare no competing financial interest.

Multifractal motif	Representative figure	Multifractal f-α curve
0.8 0.1 0.03 0.07	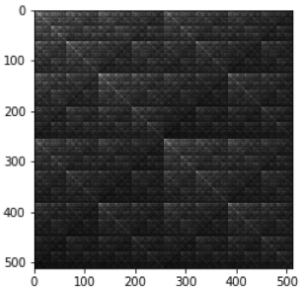 Clusters of dark pixels.	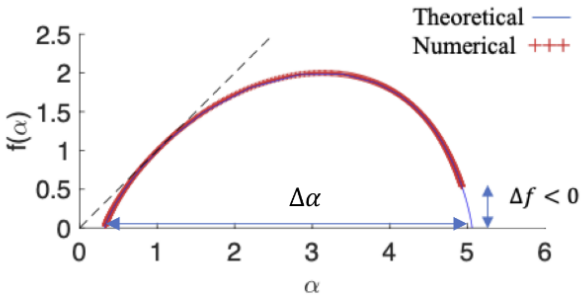 The f-α curve is skewed left and $\Delta f < 0$.
0.24 0.26 0.255 0.245	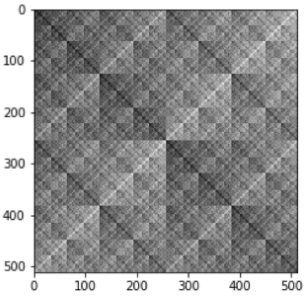 Homogeneous – no clusters.	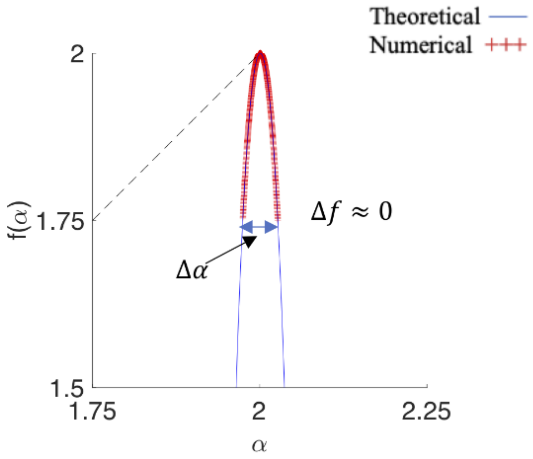 The f-α curve is not skewed and $\Delta f \approx 0$.
0.3 0.33 0.27 0.05	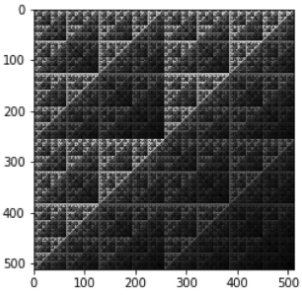 Clusters of bright pixels.	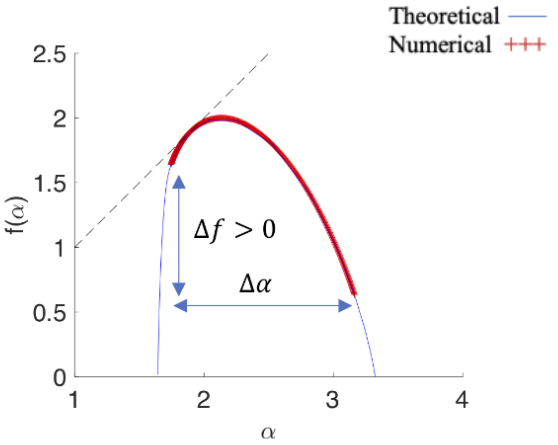 The f-α curve is skewed right and $\Delta f > 0$.

Figure 1. The theory of multifractal analysis (MFA) and $f(\alpha)$ curves.

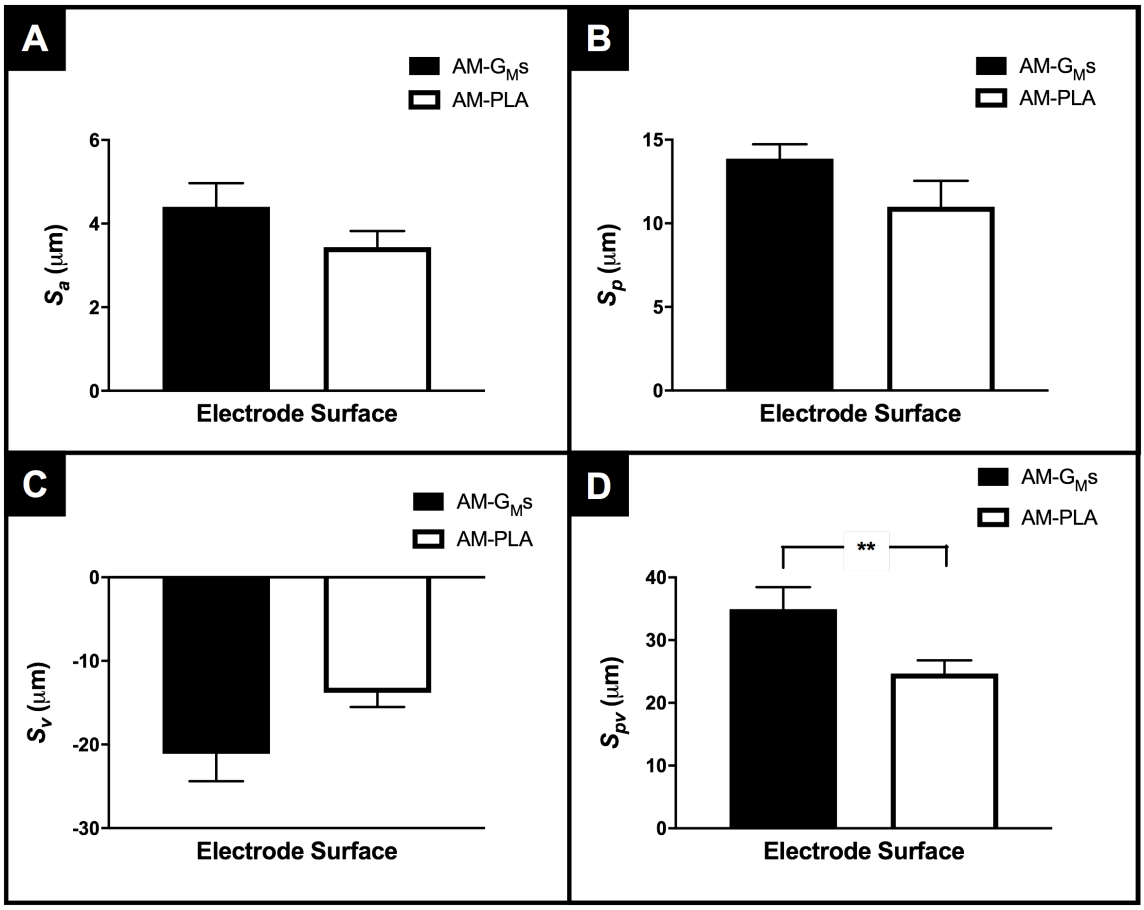

Figure 2. Optical interferometry showing surface roughness which was quantitatively defined through the measurement of values such as A) average roughness (S_a), B) highest peak (S_p), C) lowest valley (S_v) and D) peak-to-valley ratio (S_{pv}). Asterisks denote statistical significance, ** ($P \leq 0.01$) ($N = 9$).

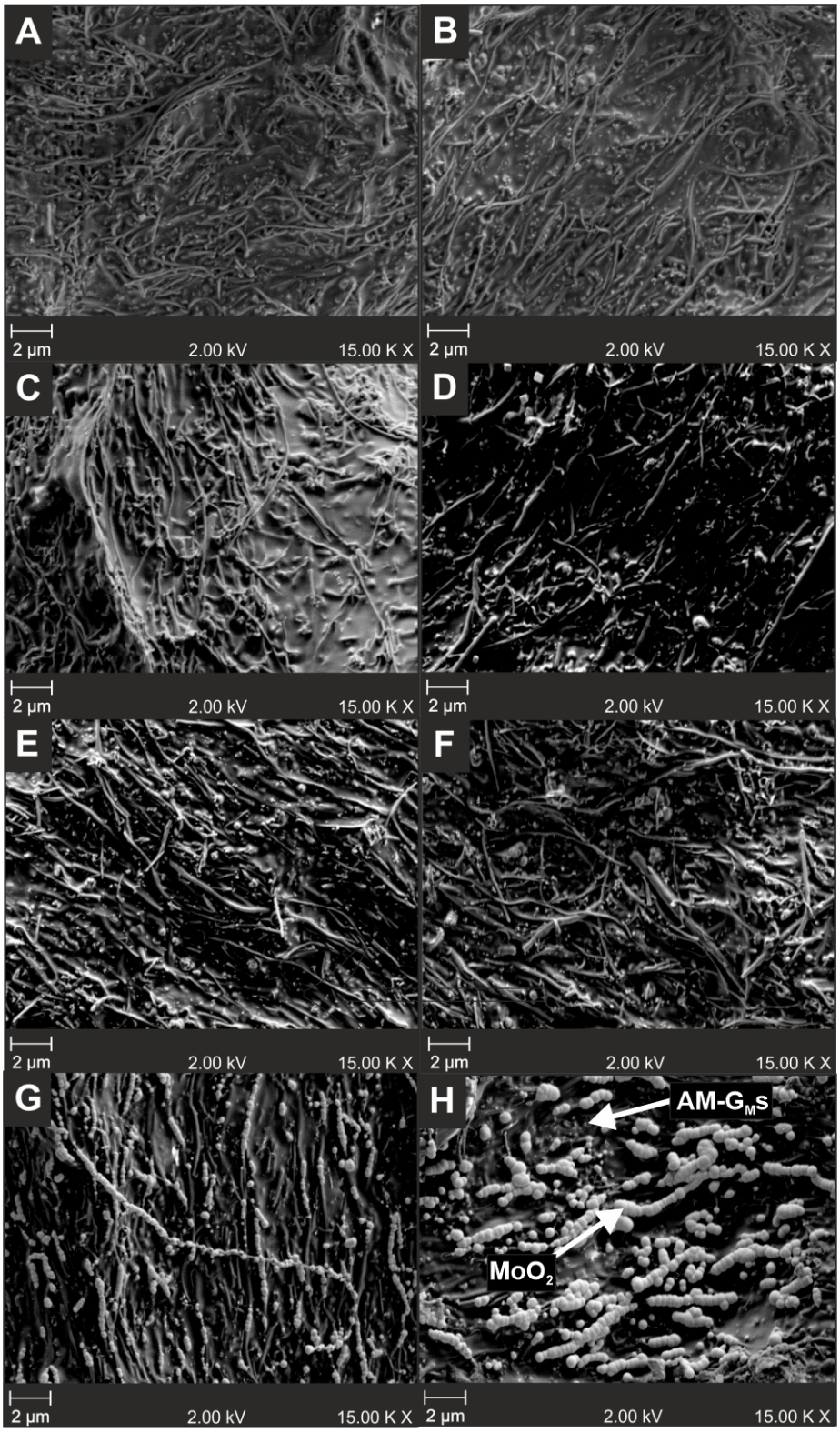

Figure 3. SEM of the surface of the AM-G_MS – showing the deposited MoO_2 A), Control, B) 20 s, C) 40 s, D) 60 s, E) 120 s, F) 180 s, G) 240 s and H) 300 s.

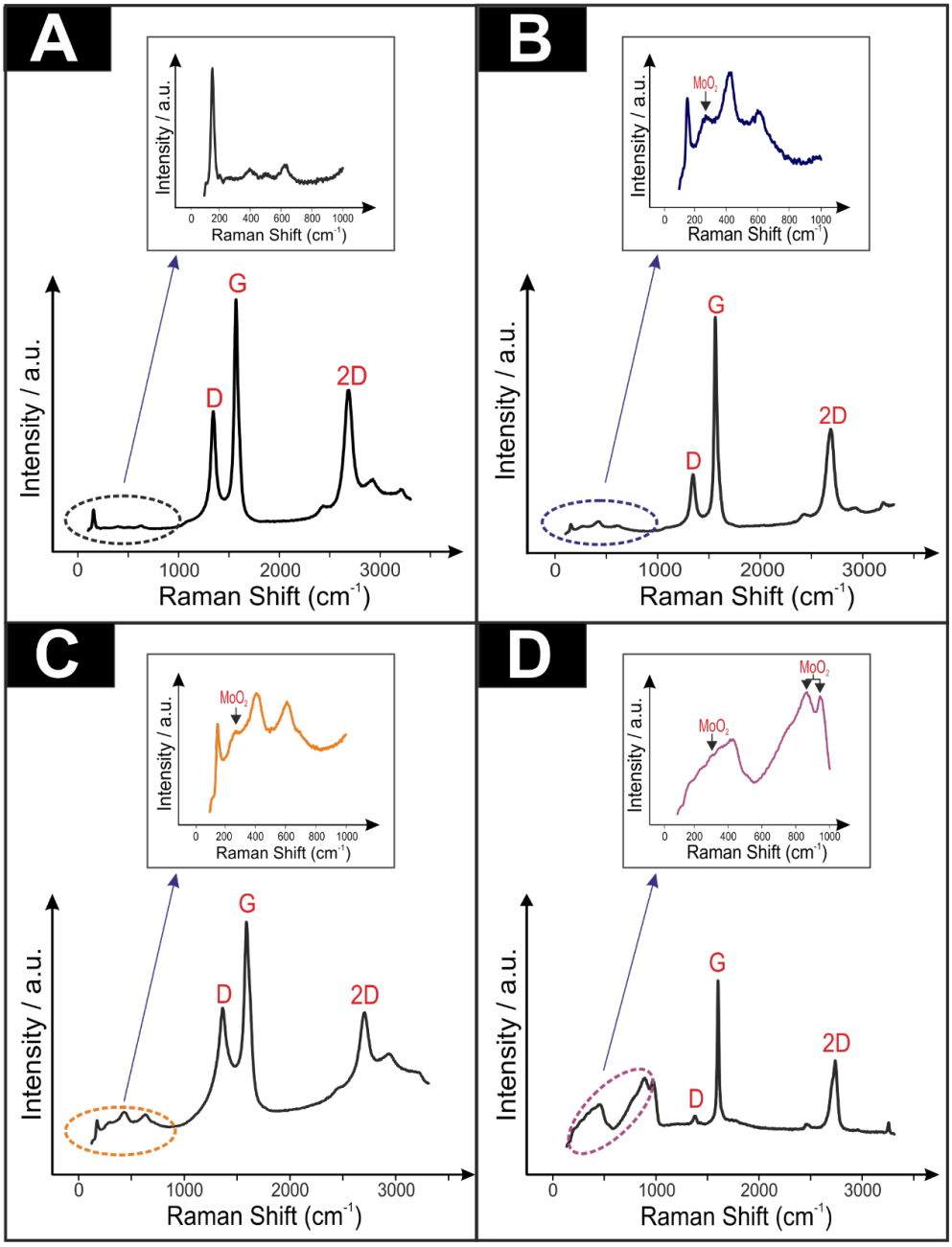

Figure 4. Selected Raman spectra of four MoO_2 deposition time points upon the AM-G_{MS}s. A) Control (black), B) 120 s (blue), C) 180 s (orange) and D) 300 s (purple). Insets focus on the first 1000 cm^{-1} where MoO_2 deposition was evident.

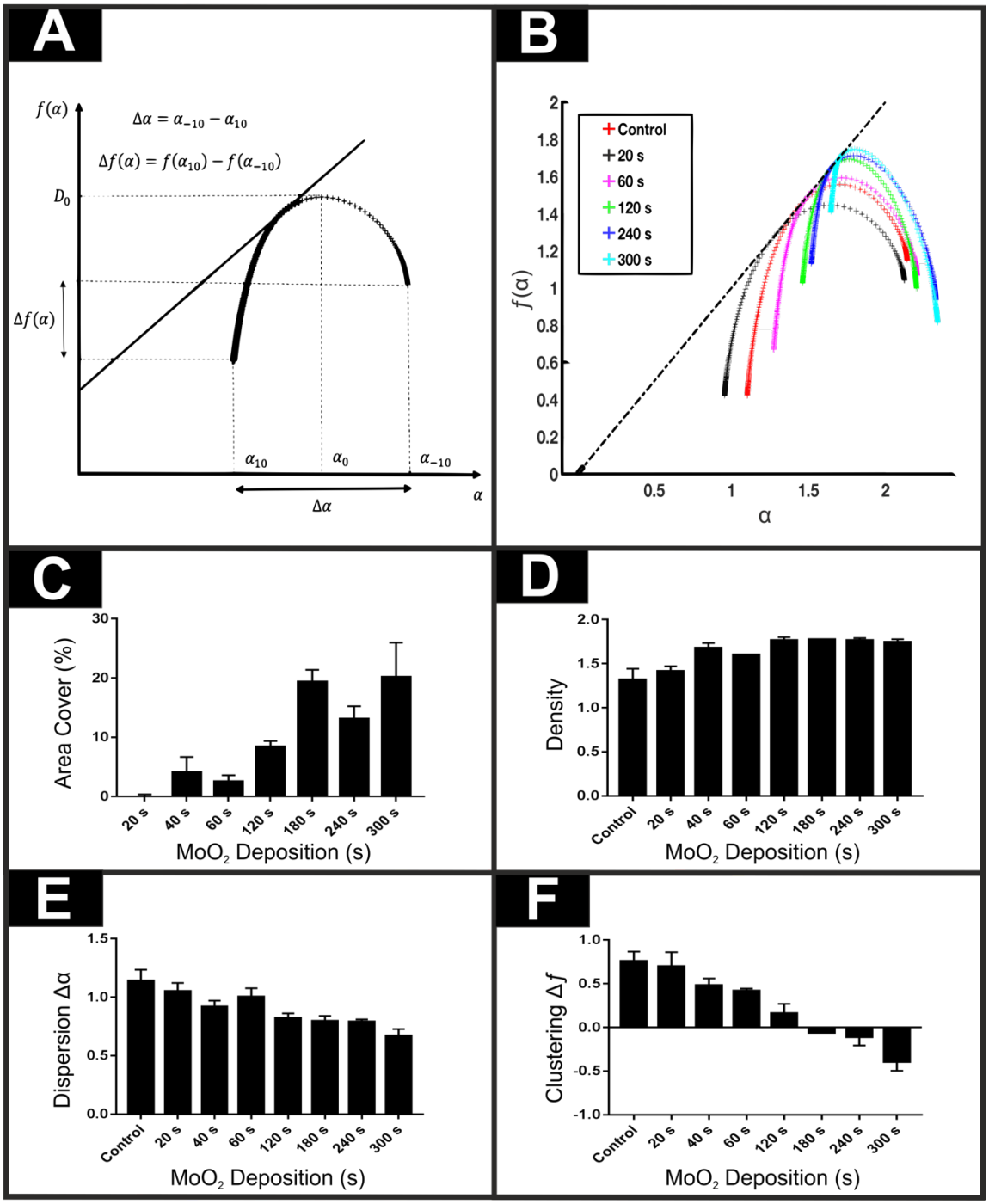

Figure 5. A) Theory of $f(\alpha)$ curves for MFA B) $f(\alpha)$ curves of a selection of MoO_2 time points selected for this study (control, 20, 60, 120, 240, 300 s) C) MoO_2 Area cover (deducted from the control background (%) D) MoO_2 Density E) MoO_2 dispersion F) MoO_2 clustering (N = 3).

Table 1. The generalized fractal dimensions (or multifractal dimensions), D_q, for the $f(\alpha)$ spectra displayed in Figure 5 B) when $-10 \leq q \leq 10$.

D_q	A) Control	B) 20s	D) 60s	E) 120s	G) 240s	H) 300s
D_{-10}	2.0509	2.0244	2.1031	2.0934	2.2016	2.2004
⋮	⋮	⋮	⋮	⋮	⋮	⋮
D_{-3}	1.8997	1.8573	1.9310	1.9251	2.0021	1.9880
D_{-2}	1.8258	1.7758	1.8525	1.8598	1.9211	1.9102
D_{-1}	1.7075	1.6396	1.7325	1.7752	1.8135	1.8191
D_0	1.5562	1.4449	1.5932	1.6936	1.7119	1.7452
D_{+1}	1.4439	1.2934	1.5099	1.6445	1.6598	1.7124
D_{+2}	1.3586	1.1891	1.4585	1.6069	1.6306	1.6988
D_{+3}	1.3087	1.1344	1.4304	1.5825	1.6153	1.6940
⋮	⋮	⋮	⋮	⋮	⋮	⋮
D_{+10}	1.1776	1.0138	1.3418	1.5098	1.5624	1.6721

References

(1) Hou, J.; Shao, Y.; Ellis, M. W.; Moore, R. B.; Yi, B. Graphene-based electrochemical energy conversion and storage: fuel cells, supercapacitors and lithium ion batteries. *Phys. Chem. Chem. Phys.* **2011**, *13*, 15384-15402.

(2) Novoselov, K. S.; Geim, A. K.; Morozov, S. V.; Jiang, D.; Zhang, Y.; Dubonos, S. V.; Grigorieva, I. V.; Firsov, A. A. Electric field effect in atomically thin carbon films. *Science* **2004**, *306*, 666-669.

(3) Jariwala, D.; Sangwan, V. K.; Lauhon, L. J.; Marks, T. J.; Hersam, M. C. Carbon nanomaterials for electronics, optoelectronics, photovoltaics, and sensing. *Chem. Soc. Rev.* **2013**, *42*, 2824-2860.

(4) Eatemadi, A.; Daraee, H.; Karimkhanloo, H.; Kouhi, M.; Zarghami, N.; Akbarzadeh, A.; Abasi, M.; Hanifehpour, Y.; Joo, S. W. Carbon nanotubes: properties, synthesis, purification, and medical applications. *Nanoscale Res. Lett*. **2014**, *9*, 393.

(5) Georgakilas, V.; Perman, J. A.; Tucek, J.; Zboril, R. Broad family of carbon nanoallotropes: classification, chemistry, and applications of fullerenes, carbon dots, nanotubes, graphene, nanodiamonds, and combined superstructures. *Chem. Rev*. **2015**, *115*, 4744-4822.

(6) Hamzah, H. H.; Shafiee, S. A.; Abdalla, A.; Patel, B. A. 3D printable conductive materials for the fabrication of electrochemical sensors: A mini review. *Electrochem. Comm.* **2018**, *96*, 27-31.

(7) Guima, K.-E.; Souza, V. H.; Martins, C. A. Insulating 3D-printed templates are turned into metallic electrodes: application as electrodes for glycerol electrooxidation. *RSC Adv.* **2019**, *9*, 15158-15161.

(8) Zhu, C.; Han, T. Y.-J.; Duoss, E. B.; Golobic, A. M.; Kuntz, J. D.; Spadaccini, C. M.; Worsley, M. A. Highly compressible 3D periodic graphene aerogel microlattices. *Nat. Comm.* **2015**, *6*, 6962.

(9) Zhang, Q.; Zhang, F.; Medarametla, S. P.; Li, H.; Zhou, C.; Lin, D. 3D printing of graphene aerogels. *Small* **2016**, *12*, 1702-1708.

(10) Foster, C. W.; Down, M. P.; Zhang, Y.; Ji, X.; Rowley-Neale, S. J.; Smith, G. C.; Kelly, P. J.; Banks, C. E. 3D printed graphene based energy storage devices. *Sci. Rep*. **2017**, *7*, 42233.

(11) Foo, C. Y.; Lim, H. N.; Mahdi, M. A.; Wahid, M. H.; Huang, N. M. Three-dimensional printed electrode and its novel applications in electronic devices. *Sci. Rep*. **2018**, *8*, 7399.

(12) Hu, X.; Zhang, W.; Liu, X.; Mei, Y.; Huang, Y. Nanostructured Mo-based electrode materials for electrochemical energy storage. *Chem. Soc. Rev*. **2015**, *44*, 2376-2404.

(13) Rajeswari, J.; Kishore, P. S.; Viswanathan, B.; Varadarajan, T. K. One-dimensional MoO_2 nanorods for supercapacitor applications. *Electrochem. Commun*. **2009**, *11*, 572-575.

(14) Li, X.; Shao, J.; Li, J.; Zhang, L.; Qu, Q.; Zheng, H. Ordered mesoporous MoO_2 as a high-performance anode material for aqueous supercapacitors. *J. Power Sources* **2013**, *237*, 80-83.

(15) Lu, X.-F.; Huang, Z.-X.; Tong, Y.-X.; Li, G.-R. Asymmetric supercapacitors with high energy density based on helical hierarchical porous Na_xMnO_2 and MoO_2. *Chem. Sci.* **2016**, *7*, 510-517.

(16) Zhou, Y.; Lee, C. W.; Yoon, S. Development of an Ordered Mesoporous Carbon/MoO_2 Nanocomposite for High Performance Supercapacitor Electrode. *Electrochem. Solid-State Lett*. **2011**,

14, 157-160.
(17) Kim, H.-S.; Cook, J. B.; Tolbert, S. H.; Dunn, B. The Development of Pseudocapacitive Properties in Nanosized-MoO_2. *J. Electrochem*. **2015**, *162*, 5083-5090.
(18) Rowley-Neale, S. J.; Brownson, D. A. C.; Smith, G. C.; Sawtell, D. A. G.; Kelly, P. J.; Banks, C. E. 2D nanosheet molybdenum disulphide (MoS_2) modified electrodes explored towards the hydrogen evolution reaction. *Nanoscale* **2015**, *7*, 18152-18168.
(19) Galdino, F. E.; Foster, C. W.; Bonacin, J. A.; Banks, C. E. Exploring the electrical wiring of screen-printed configurations utilised in electroanalysis. *Anal. Methods* **2015**, *7*, 1208-1214.
(20) Musameh, M.; Notivoli, M. R.; Hickey, M.; Huynh, C. P.; Hawkins, S. C.; Yousef, J. M.; Kyratzis, I. L. Carbon nanotube-Web modified electrodes for ultrasensitive detection of organophosphate pesticides. *Electrochim. Acta* **2013**, *101*, 209-215.
(21) Subramanian, R.; Lakshminarayanan, V. Effect of adsorption of some azoles on copper passivation in alkaline. *Corros. Sci.* **2002**, *44*, 535-554.
(22) Walter, E. C.; Zach, M. P.; Favier, F.; Murray, B. J.; Inazu, K.; Hemminger, J. C.; Penner, R. M. Metal nanowire arrays by electrodeposition. *Chem. Phys. Chem.* **2003**, *4*, 131-138.
(23) Slate, A. J.; Wickens, D.; Wilson-Nieuwenhuis, J.; Dempsey-Hibbert, N.; West, G.; Kelly, P.; Verran, J.; Banks, C. E.; Whitehead, K. A. The effects of blood conditioning films on the antimicrobial and retention properties of zirconium-nitride silver surfaces. *Colloid Surface B* **2019**, *173*, 303-311.
(24) Randviir, E. P.; Brownson, D. A. C.; Metters, J. P.; Kadara, R. O.; Banks, C. E. The fabrication, characterisation and electrochemical investigation of screen-printed graphene electrodes. *Phys. Chem. Chem. Phys*. **2014**, *16*, 4598-4611.
(25) Wickens, D.; Lynch, S.; West, G.; Kelly, P.; Verran, J.; Whitehead, K. A. Quantifying the pattern of microbial cell dispersion, density and clustering on surfaces of differing chemistries and topographies using multifractal analysis. *J. Microbiol. Methods* **2014**, *104*, 101-108.
(26) Moreira, J.; Gomes, L.; Whitehead, K.; Lynch, S.; Tetlow, L.; Mergulhão, F. Effect of surface conditioning with cellular extracts on *Escherichia coli* adhesion and initial biofilm formation. *Food Bioprod. Process.* **2017**, *104*, 1-12.
(27) Zach, M. P.; Ng, K. H.; Penner, R. M. Molybdenum nanowires by electrodeposition. *Science* **2000**, *290*, 2120-2123.
(28) Rowley-Neale, S. J.; Brownson, D. A.; Banks, C. E. Defining the origins of electron transfer at screen-printed graphene-like and graphite electrodes: MoO_2 nanowire fabrication on edge plane sites reveals electrochemical insights. *Nanoscale* **2016**, *8*, 15241-15251.
(29) Ferrari, A. G.-M.; Foster, C. W.; Brownson, D. A.; Whitehead, K. A.; Banks, C. E. The influence of lateral flake size in graphene/graphite paste electrodes: an electroanalytical investigation. *Sci. Rep*. **2019**, *9*, 1-9.
(30) Ferrari, A. C. Raman spectroscopy of graphene and graphite: Disorder, electron–phonon coupling, doping and nonadiabatic effects. *Solid State Commun.* **2007**, *143*, 47-57.

(31) Graf, D.; Molitor, F.; Ensslin, K.; Stampfer, C.; Jungen, A.; Hierold, C.; Wirtz, L. Spatially resolved raman spectroscopy of single- and few-layer graphene. *Nano Lett.* **2007**, *7*, 238-242.
(32) Wang, Y. Y.; Ni, Z. H.; Yu, T.; Shen, Z. X.; Wang, H. M.; Wu, Y. H.; Chen, W.; Shen Wee, A. T. Raman studies of monolayer graphene: the substrate effect. *J. Phys. Chem. C* **2008**, *112*, 10637-10640.
(33) Yoon, D.; Moon, H.; Cheong, H.; Choi, J. S.; Choi, J. A.; Park, B. H. Variations in the raman spectrum as a function of the number of graphene layers. *J. Korean Phys. Soc* **2009**, *55*, 1299-1303.
(34) Kondratowicz, I.; Żelechowska, K.; Majdecka, D.; Bilewicz, R. Synthesis and modification of reduced graphene oxide aerogels for biofuel cell applications. Mater. Sci-Poland **2015**, 33, 292-300.
(35) Reich, S.; Thomsen, C. Raman spectroscopy of graphite. *Philos. T. R. Soc. A* **2004**, *362*, 2271-2288.
(36) Casiraghi, C.; Hartschuh, A.; Qian, H.; Piscanec, S.; Georgi, C.; Fasoli, A.; Novoselov, K.; Basko, D.; Ferrari, A. Raman spectroscopy of graphene edges. *Nano Lett*. **2009**, *9*, 1433-1441.
(37) Kim, K.; Coh, S.; Tan, L. Z.; Regan, W.; Yuk, J. M.; Chatterjee, E.; Crommie, M.; Cohen, M. L.; Louie, S. G.; Zettl, A. Raman spectroscopy study of rotated double-layer graphene: misorientation-angle dependence of electronic structure. *Phys. Rev. Lett*. **2012**, *108*, 246103.
(38) Lin, Z.; Ye, X.; Han, J.; Chen, Q.; Fan, P.; Zhang, H.; Xie, D.; Zhu, H.; Zhong, M. Precise control of the number of layers of graphene by picosecond laser thinning. *Sci. Rep*. **2015**, *5*, 11662.
(39) Zhou, E.; Wang, C.; Zhao, Q.; Li, Z.; Shao, M.; Deng, X.; Liu, X.; Xu, X. Facile synthesis of MoO_2 nanoparticles as high performance supercapacitor electrodes and photocatalysts. *Ceram. Int*. **2016**, *42*, 2198-2203.
(40) Tetlow, L. A.; Lynch, S.; Whitehead, K. A. The effect of surface properties on bacterial retention: A study utilising stainless steel and TiN/25.65 at.% Ag substrata. *Food Bioprod. Process*. **2017**, *102*, 332-339.
(41) Lopes, R.; Betrouni, N. Fractal and multifractal analysis: a review. *Med. Image Anal.* **2009**, *13*, 634-649.
(42) Amin, M.; Rowley-Neale, S. J.; Shalamanova, L.; Lynch, S.; Wilson-Nieuwenhuis, J.; El Mohtadi, M.; Banks, C. E.; Whitehead, K. A. Molybdenum disulfide surfaces to reduce *Staphylococcus aureus* and *Pseudomonas aeruginosa* biofilm formation. *ACS Appl. Mater. Interfaces* **2020**, *12*, 21057-21069.
(43) Gutfraind, R.; Sheintuch, M.; Avnir, D. Fractal and multifractal analysis of the sensitivity of catalytic reactions to catalyst structure. *J. Chem. Phys*. **1991**, *95*, 6100-6111.
(44) Ţălu, S. t.; Stach, S.; Ghodselahi, T.; Ghaderi, A.; Solaymani, S.; Boochani, A.; Garczyk, Z. A. Topographic characterization of Cu–Ni NPs @ a-C:H films by afm and multifractal analysis. *J. Phys. Chem.* B **2015**, *119*, 5662-5670.
(45) Salat, H. P. P.; Murcio Villanueva, R.; Arcaute, E. Multifractal methodology. *Physica A* **2017**, *473*, 467-487.

ToC Graphic

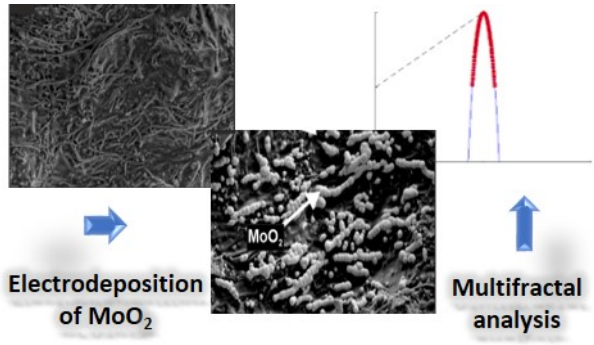

Electronic Supplementary Information (ESI):

Electrochemical Decoration of Additively Manufactured Graphene Macroelectrodes with MoO_2 Nanowires: An Approach to Demonstrate the Surface Morphology

Anthony J. Slate[1,2,3], Kathryn A. Whitehead[1,3]*, Stephen Lynch[4], Christopher W. Foster[1], and Craig E. Banks[1,2]*

[1]: Faculty of Science and Engineering, Manchester Metropolitan University, Chester Street, Manchester, M1 5GD, UK.

[2]: Manchester Fuel Cell Innovation Centre, Manchester Metropolitan University, Chester Street, Manchester M1 5GD, UK.

[3]: Microbiology at Interfaces, Department of Life Sciences, Manchester Metropolitan University, Chester Street, Manchester M1 5GD, UK.

[4]: *Department of Computing and Mathematics, Manchester Metropolitan University, Chester Street, Manchester M1 5GD, UK*

The Journal of Physical Chemistry C

*To whom correspondence should be addressed.

Email: K.A.Whitehead@mmu.ac.uk (Proofs and correspondence); c.banks@mmu.ac.uk

Figure S1. Raman spectra of the eight MoO_2 deposition time points against the AM-G_Ms. A) Control (black), B) 20 s (blue), C) 40 s (green), D) 60 s (grey), E) 120 s (dark blue), F) 180 s (orange), G) 240 s (red) and H) 300 s (purple).

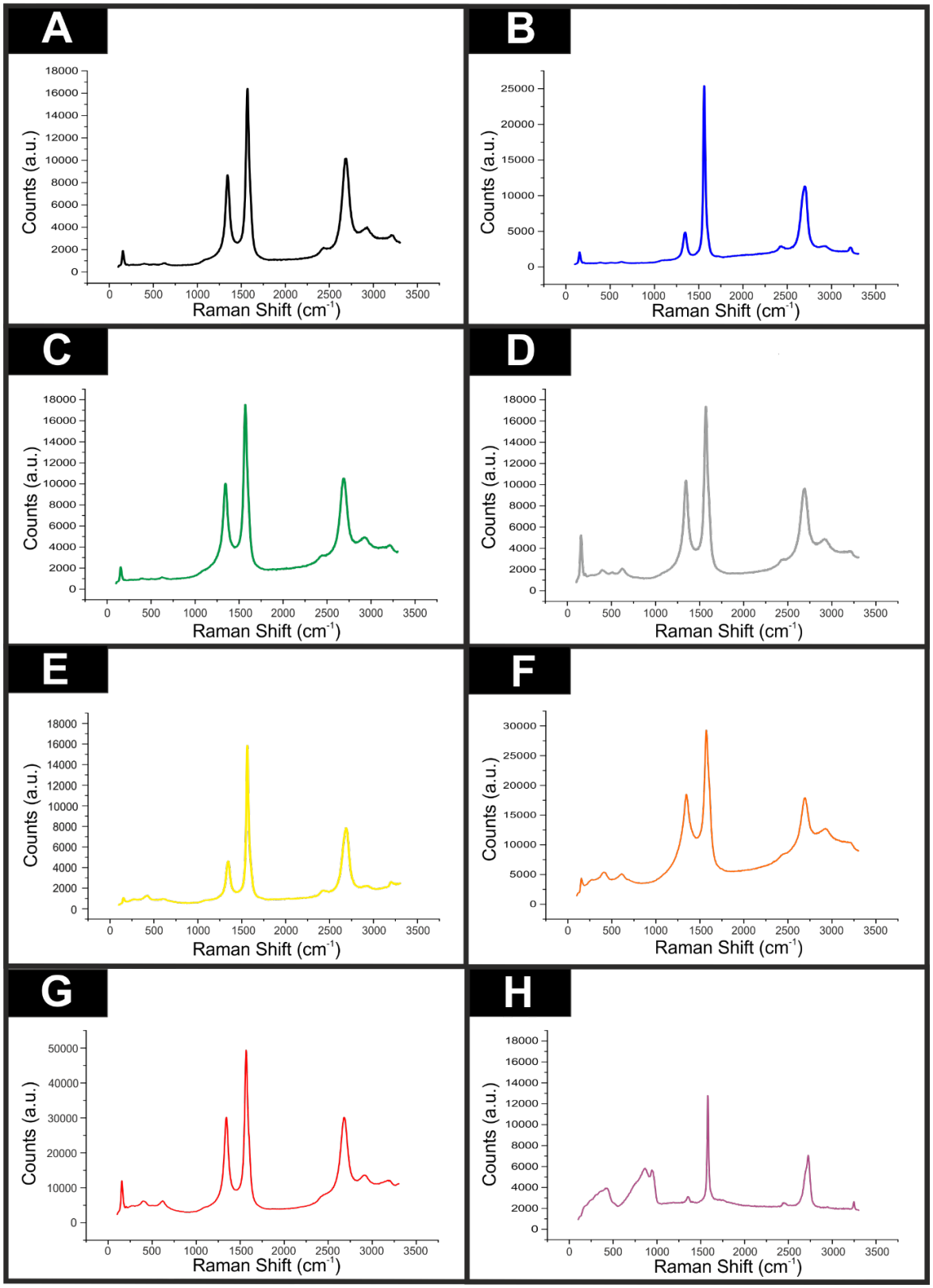
A
B
C
D
E
F
G
H
Counts (a.u.)
Raman Shift (cm-1)

Figure S2. Raman spectra (focussing on the first 1000 cm^{-1}) of the eight MoO2 deposition time points against the AM-G_{MS}s. A) Control (black), B) 20 s (blue), C) 40 s (green), D) 60 s (grey), E) 120 s (dark blue), F) 180 s (orange), G) 240 s (red) and H) 300 s (purple).

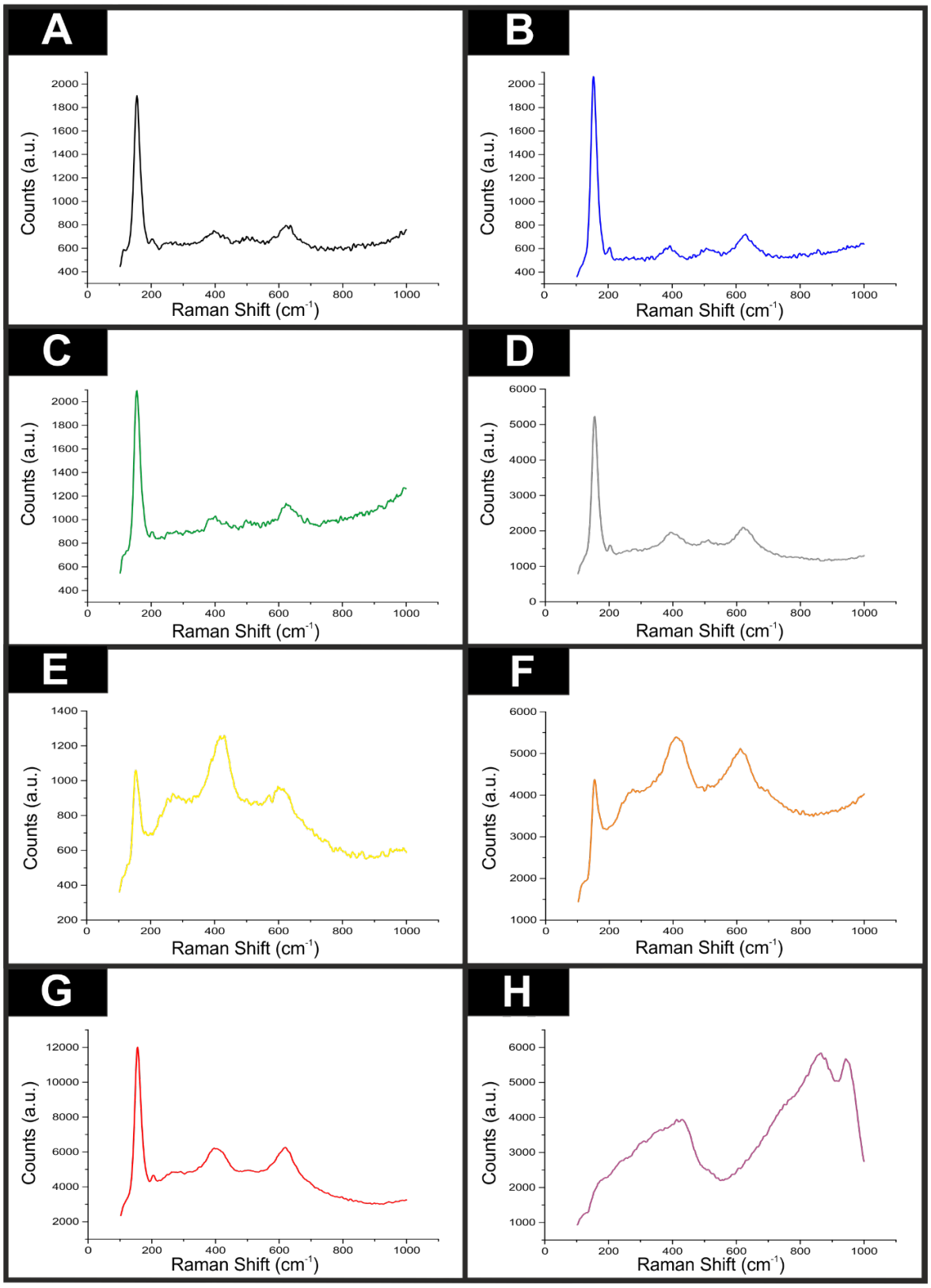

Figure S3. Examples of the binary images, which were generated and modified following SEM, before MFA was conducted. A) Control, B) 20 s, C) 40 s, D) 60 s, E) 120 s, F) 180 s, G) 240 s and H) 300 s.